2013 European Control Conference (ECC)
July 17-19, 2013, Zürich, Switzerland.

Estimation of the distributed temperature of a SI engine catalyst for light-off strategy

Delphine Bresch-Pietri, Thomas Leroy, Nicolas Petit

Abstract— **This paper proposes a model for the internal temperature of a SI engine catalyst, aiming at designing a prediction-based light-off strategy. Due to its elongated geometry where a gas stream is in contact with a spatially distributed monolith, the system under consideration is inherently a distributed parameter system. This paper advocates an approach which is based on a one-dimensional distributed parameter model, coupled with an advection-diffusion equation accounting for the distributed heat generation resulting from pollutant conversion. Following recent works, this heat supply is shown here to be equivalent to an inlet temperature entering the system at a virtual entry point inside the catalyst. This new input has a static gain depending on the state of the system, which introduced a coupling. Taking advantage of the low-pass filter characteristic of the system, an estimate of this model is designed and results into a time-varying input-delay system whose dynamics parameters (time constant, delay, gains) are obtained through a simple analytic reduction procedure. A corresponding prediction-based light-off strategy is proposed and illustrated in simulations exploiting experimental data.**

I. Introduction

Automotive SI engines are equipped with a Three-Way Catalyst (TWC) located in the exhaust line. This after-treatment device aims at reducing the three major pollutants resulting from the combustion: hydrocarbons HC, carbon monoxide CO and nitrogen oxide NO_x. Yet, conversion efficiency highly depends on the catalyst temperature [8] [9], as presented in Fig. 5. In this context, a cold start of the engine is problematic, as the temperature is too low to activate chemical reactions. As a result, the catalyst conversion ratio is poor [17] and pollutant emissions are above admissible levels. Therefore, speed-up of the catalyst warm-up is a point of critical importance.

When the catalyst is cold, heat source is provided by the exhaust burned gas, which, flowing through the monolith, are exchanging with the layer and warming it. Therefore, active warm-up strategies classically aim at feeding the catalyst with gas having higher temperature, exploiting combustion timing shifting [7]. This open-loop technique relies on combustion efficiency degradation which, in turn, to satisfy the driver torque request, yields substantial consumption increase. To limit this negative effect of the open-loop strategy, it is of prime importance to determine when the catalyst should reach its light-off temperature[1]. This would generate a satisfactory compromise between pollutant emissions and consumption. When this light-off temperature is obtained, optimal combustion can be performed and the consumption can simply go back to a standard level.

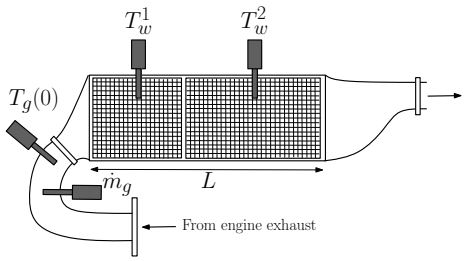

Fig. 1. Experimental catalyst composed of two monoliths. Two sensors permit to measure the wall temperature in the center of each monolith. Test-bench is also equipped with inlet temperature and mass flow sensors.

Unfortunately, no temperature sensor is available on commercially embedded catalysts. The switch time is usually determined from the measurements provided by a temperature sensor located into the cooling system. Certainly, the thermal behavior of the water cooling system can be indirectly related to the engine and exhaust line temperatures. Yet, this information is relatively uncertain (and lags behind), as other sources of heat can bias it. Under realistic driving conditions, this reference water temperature, optimized for one particular normalized cycle (e.g. NEDC or FTP), can be completely uncorrelated with the catalyst light-off. This may lead either to higher consumption (if the light-off is estimated too late) or to higher pollutant emissions (if the light-off is estimated too soon).

To avoid such a bad detection, an alternative is to rely on models, accounting for the inherent distributed nature of the catalyst and the intrinsic transport phenomenon. Some infinite-dimensional model have been proposed in [11], [14] or [4], under the form of Partial Differential Equations (PDE), modeling heat exchange and chemistry inside the monolith. These models give very accurate estimation of the light-off temperature, but introduce very complex representations of the heat release by chemical reactions. Further, the induced computational burden discards them from real-time implementations.

Some alternative catalyst temperature models have been proposed. In [10], a mean-value (spatially lumped) model

D. Bresch-Pietri is with the Department of Mechanical Engineering, MIT, Cambridge, MA 02139 *Email : dbp@mit.edu*

T. Leroy is with the Département Contrôle, Signal et Système in IFP Energies nouvelles, 1-4 Av. du Bois Préau, 92852 Rueil Malmaison, France

N. Petit is with the Centre Automatique et Systèmes, Unité Mathématiques et Systèmes at MINES ParisTech, 60 Bd St Michel, 75272 Paris, France

[1]Defined here as the temperature at which the catalyst becomes more than 90 percent effective.

is presented, in which the catalyst temperature follows a first-order dynamics, assuming the temperature inside the wall temperature as spatially homogeneous. This kind of model is known to be inaccurate, as it usually leads to an overestimation of the light-off temperature.

In this paper, following the overture presented in [12], we propose to represent the chemical reactions inside the catalyst as a temperature entering the system at a virtual entry point located downstream of the physical inlet of the monolith. To make this approach compliant with SI engines applications, it is proposed here to use the catalyst efficiency conversion to calculate the gain relating the heat release to the fictitious temperature. As this efficiency depends on the output of the model, it introduces an additional coupling, which is shown here not to be detrimental to the stability of the model. The validity of this PDE model is emphasized on experimental data.

Besides, these PDE equations are exploited to propose a semi-lumped model, under the form of a first-order input-delay dynamics relating the inlet gas temperature to any punctual wall catalyst temperature. The accuracy of this model, of gentle implementation complexity, is discussed at the light of experimental data. Taking advantage of the delayed nature of the model, a corresponding open-loop prediction-based light-off control strategy is proposed and illustrated with simulations. This is the main contribution of the paper.

The paper is organized as follows. In Section II, we give main context elements and present the catalyst under consideration in experiments. In Section III, we detail the PDE temperature modeling which is used in Section IV to derive a first-order input-delay model through analytic formula stemming from simple operational calculus. Finally, in Section V, we detail a corresponding open-loop prediction-based light-off strategy of the catalyst, illustrated by simulations.

II. Experimental set-up

The catalyst under consideration in this study is mounted at the outlet of a 2L four-cylinder turbocharged SI engine, downstream the turbine. Fig. 1 presents a scheme of the catalyst under consideration. It is composed of two separated monoliths [18] in charge of oxidizing carbon monoxides and hydrocarbons into carbon dioxide and water, and reducing nitrogen oxides to nitrogen and oxygen[2]. For experimental studies and comparisons, the catalyst has been instrumented with two internal temperature sensors. Such sensors are not embedded on any commercial line product and serve here for providing experimental data only. Fig. 2 presents experimental results obtained at test bench during a NEDC (New European Driving Cycle) cycle. Histories of both the exhaust mass flow and the temperature located upstream the catalyst are reported in Fig. 2(a). These quantities are the inputs of the

[2]In the following, the two monoliths are not distinguished. In details, neglecting the conduction inside the wall catalyst yields to the equivalent representation of a unique monolith.

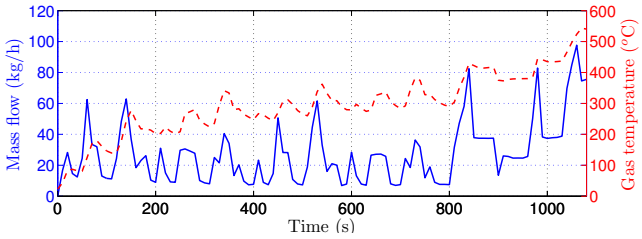

(a) Exhaust gas flow (solid line) and temperature (dashed line).

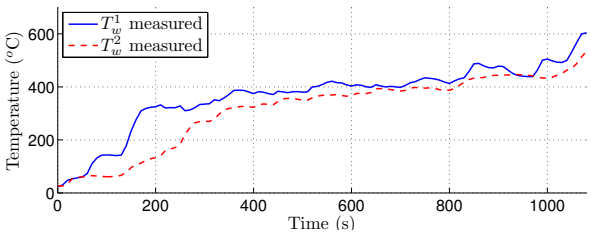

(b) First and second monolith temperature.

Fig. 2. Experimental results on European driving cycle (NEDC).

model proposed in this paper. The exhaust mass flow is a fast-varying variable closely related to the engine torque output. The exhaust temperature has a slower dynamics because of the pipes thermal inertia. In Fig. 2(b), both monolith temperatures of Fig. 1 are given[3]. By comparing these two curves between them and against the inlet gas temperature, one can easily see the impact of the catalyst thermal inertia since it deeply slows down the temperature response inside the monoliths. The distributed nature of the catalyst is then conspicuous. A second important point to notice is the visible very low-pass filter role of the catalyst (see the signals Tw^1 and T_w^2 on Fig. 2(b)). We will account for this in Section IV.

III. PDEs model representation

We now refer to Fig. 3, where a schematic representation of the monolith is given. Exhaust burned gas enter the monolith at $x = 0$ and convective exchanges with the wall occur all along the monolith, i.e. for $x = 0$ to $x = L$, yielding to non-uniform distributed temperature profiles of the gas $T_g(x,t)$ and the catalyst wall $T_w(x,t)$[4]. Chemical reactions

[3]The presented results are obtained by performing the combustion with greatest efficiency during the whole cycle, without warm-up strategy. The duration of the warming phase is therefore longer than a classical one.

[4]On the contrary, the axial conduction in the solid is not important and can be neglected, as underlined in [19], [20]

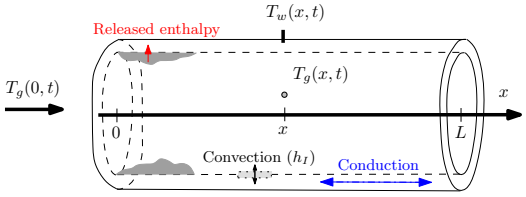

Fig. 3. Schematic view of the distributed profile temperature inside a catalyst jointly with thermal exchanges.

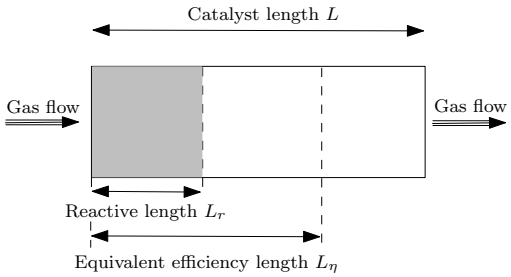

Fig. 4. Schematic view inspired from [12]. The conversion is assumed to take place on an upstream part of the catalyst of length L_r. The temperature used to determine the catalyst efficiency is located at length $L_\eta \leq L$.

occur distributely along the monolith, depending on the wall temperature profile.

A. Complete model

We consider the following coupled linear infinite dimensional thermal dynamics

$$\begin{cases} \dfrac{\partial T_w}{\partial t}(x,t) = k_1(T_g(x,t) - T_w(x,t)) + \Psi(x,t,T_w(x,t)) & (1) \\ \dot{m}_g \dfrac{\partial T_g}{\partial x}(x,t) = k_2(T_w(x,t) - T_g(x,t)) & (2) \end{cases}$$

with the boundary conditions $\frac{\partial T_w}{\partial x}(0,t) = \frac{\partial T_w}{\partial x}(L,t) = 0$, $T_g(0,t)$ given and where ψ is a distributed time-varying source term, related to the chemical reaction occurring inside the catalyst and the constants $k_1, k_2 > 0$ are defined as

$$k_1 = \frac{h_I P_I}{A_w \rho_w C p_w}, \quad k_2 = \frac{h_I P_I}{C p_g}$$

Such a model is considered for example in [11]. It encompasses the detailed modeling (13)-(14) given in Appendix, provided that a few simplifications are performed:

- conduction ($\lambda_w \partial^2 T_g / \partial x^2$) into the monolith is neglected compared to convection exchanges;
- gas storage is considered as very small compared to the monolith one, i.e. $\rho_g C p_g << \rho_w C p_w$;
- convective exchanges with the atmosphere are neglected compared to the one with the exhaust gas[5].

B. Proposed reduced PDE model

Here, we consider that the source term ψ, which gathers the sum of the enthalpies of the various reactions taking place inside the catalyst, is uniform over some spatial interval

$$\Psi(x,t,T_w) = \begin{cases} \psi(t,T_w) & \text{for} \quad 0 \leq x \leq L_r(\dot{m}_g) \\ 0 & \text{for} \quad L_r(\dot{m}_g) < x \leq L \end{cases}$$

where L_r is the length of the portion of the catalyst where the heat is released, which is a piecewise affine function of the channel gas mass flow rate. This model is illustrated in Fig. 4. This source term also depends on the wall temperature. This point is important to study the light-off process. For moderate temperature, the conversion efficiency highly depends on the wall temperature and this dependence cannot reasonably be neglected.

a) Conversion efficiency representation: in this paper, we propose to represent the conversion efficiency of the catalyst as a function of a punctual wall temperature, at a position L_η (potentially varying with aging)[6]. Experimental determination of an appropriate length L_η and of the resulting efficiency was performed and follows the tendency of Fig. 5. In the following, the conversion efficiency is called η and is considered as a known function.

[5]This last assumption is only made for sake of simplicity in the following analysis and can easily be relaxed.

[6]At a given time, the variation of L_η modifies the sharpness of the conversion efficiency variations with respect to temperature and therefore the accuracy of the estimated efficiency. In details, the lower L_η is, the sharper the conversion efficiency variations are. While device aging, it can be expected that L_η should be increased to account for deterioration of an upstream part of the catalyst.

Symbol	Description	Unit
A_w	Catalyst wall area	m^2
A_g	Catalyst efficient area	m^2
Cp_w	Catalyst wall heat capacity	J/kg/m^3
Cp_g	Gas heat capacity	J/kg/m^3
D	Model delay	s
ΔH_{HC}	Unity enthalpy from HC conversion	J/mol
ΔH_{CO}	Unity enthalpy from CO conversion	J/mol
ΔH_{NOx}	Unity enthalpy from NO_x conversion	J/mol
h_I	Internal convection coefficient	J/K/m^2
h_O	External convection coefficient	J/K/m^2
h_i	Enthalpy of the i^{th} species reaction	J
λ_w	Wall conduction coefficient	J/K/m^2
$\dot{m}_g$	Gas mass flow rate	kg/s
P_I	Internal catalyst perimeter	m
P_O	External catalyst perimeter	m
R_i	Reaction rate of the i^{th} species	-
ρ_w	Catalyst wall volumetric mass	kg/m^3
T_w	Distributed monolith temperature	K
T_w^1	Wall temperature in the middle of the first monolith	K
T_w^2	Wall temperature in the middle of the second monolith	K
T_g	Distributed gas temperature	K
τ	Model time constant	s

TABLE I
NOTATIONS

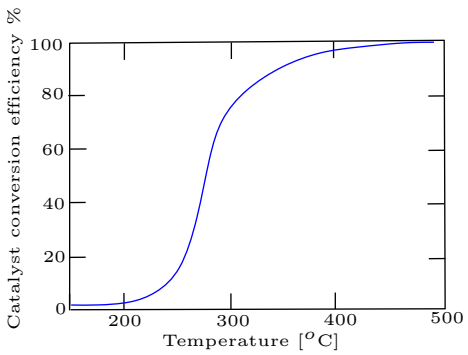

Fig. 5. Conversion efficiency (jointly for CO, HC and NO_x) as a function of temperature for typical catalytic converter (Source : [8]).

b) Virtual temperature inlet accounting for heat release: to represent the source term ψ, we propose to consider the pollutant conversion effects as a second temperature front T_{eq} occurring at the virtual position L_r inside the catalyst [7]. Indeed, for steady-state conditions, energy balance for the system can be written as

$$\dot{m}_g Cp_g \underbrace{(T_g(0) - T_g(L))}_{\triangleq T_{eq}} + \eta(T_w(L_\eta)) \sum_{i=1}^{N} \Delta H_i [x_i]_{in} = 0$$

where $[x_i]_{in}$ are the inlet pollutant concentrations. Typically, three main pollutants are considered ($N = 3$), i.e. hydrocarbons (HC), carbon monoxide (CO) and nitrogen oxides (NO_x). They result in three steady-state gains

$$G_{HC} = \eta(T_w(L_\eta)) \frac{\Delta H_{HC}}{\dot{m}_g Cp_g}, \quad G_{CO} = \eta(T_w(L_\eta)) \frac{\Delta H_{CO}}{\dot{m}_g Cp_g}$$

$$\text{and} \quad G_{NO_x} = \eta(T_w(L_\eta)) \frac{\Delta H_{NO_x}}{\dot{m}_g Cp_g}$$

where the unity enthalpy $\Delta H_{HC}, \Delta H_{CO}$ and ΔH_{NO_x} are known constants. These gains are then used to calculate an equivalent temperature

$$T_{eq} = G_{HC}[HC]_{in} + G_{CO}[CO]_{in} + G_{NO_x}[NO_x]_{in} \qquad (3)$$

In practice, the pollutant concentrations are not measured but can be effectively estimated, e.g. by look-up tables.

An important point to notice is the appearance of the temperature at length L_η as a parametrization of the conversion efficiency η. This yields a coupling represented in Fig. 6 under a closed-loop form.

Exploiting the linearity of the dynamic through a superposition principle, we propose to distinguish the $T_g(0)$ effects from the pollutant conversion effect. The distributed temperature of the catalyst is then modeled as the sum of two similar and relatively simple advection-diffusion equations of type (1)-(2) without source term (i.e. $\Psi = 0$). The propagation phenomena occurs on two different lengths. This model is represented in Fig. 6.

C. Model validation from experimental data

Simulation results of the wall catalyst temperature model at two positions (described in Fig. 1) are provided in Fig. 7 (in black) and compared to experimental measurements (in blue). These measurements were obtained on a NEDC cycle, with an initially cold catalyst. The inputs used for the models (gas mass flow rate and gas inlet temperature) are pictured in Fig. 2(a). PDEs have been implemented with an explicit numerical scheme and a sampling time $Ts = 1ms$. All parameters involved have been identified in simulation, in accordance with the literature[8].

[7] In details, this fictitious length does not exactly match the physical non-reactive length introduced earlier. Yet, for sake of simplicity, we assume here that they are identical.

[8] The proposed model was calibrated using experimental data for different given operating points, for which the engine was initially cold and requested torque and engine speed were kept constant.

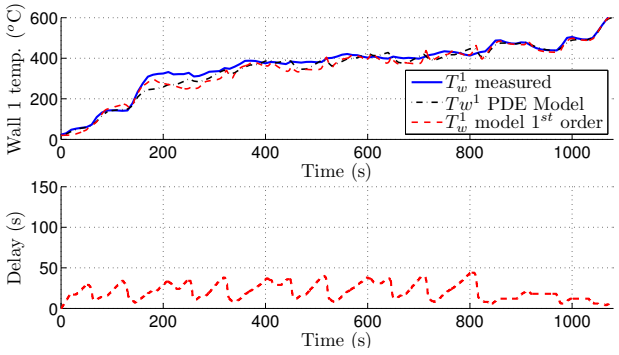

(a) Simulation results for both the proposed reduced PDE model and its approximation by an input-delay model, compared to experimental data in the center of the first monolith. Below : the corresponding delay used in the input-delay model.

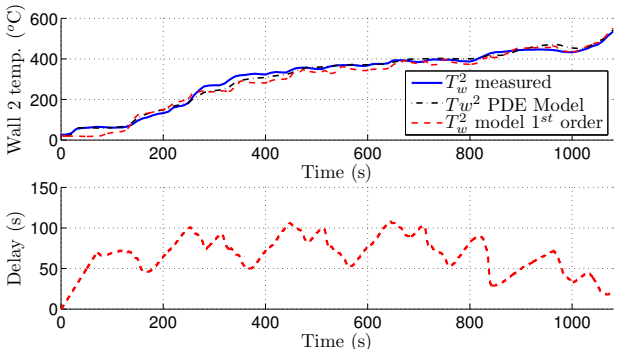

(b) Simulation results for both the proposed reduced PDE model and its approximation by an input-delay model, compared to experimental data in the center of the second monolith. Below : the corresponding delay used in the input-delay model.

Fig. 7. Comparison for a NEDC cycle between the proposed PDE model, its reduction to an input-delay system and experimental data at two location inside the monolith.

One can easily notice that the computed temperatures catch both short-term and long-term variations of the true signals, which validates the proposed distributed model.

D. Comments about the proposed model

The proposed PDE model provides accurate estimation of the wall catalyst temperature (only) on the spatial interval $[L_r, L]$, i.e. over the non-reactive length of the catalyst. For designing a light-off strategy, this is the spatial interval we are interested in.

To feed the model, values for various inputs, presented in Fig.6, are necessary: the mass flow rate, the inlet gas temperature and the pollutant emissions upstream of the catalyst. In practice, the information of the mass flow rate is given by a model already implemented for combustion control purposes (namely, cylinder charge estimation). Further, a certain number of inlet gas temperature models have been proposed in the literature and can be used here if no sensor is available. For example, the interested reader can refer to [6] where a complex 1D model is presented or to [5] for lumped parameters exhaust temperature models.

We are interested in the design of a simple model of the

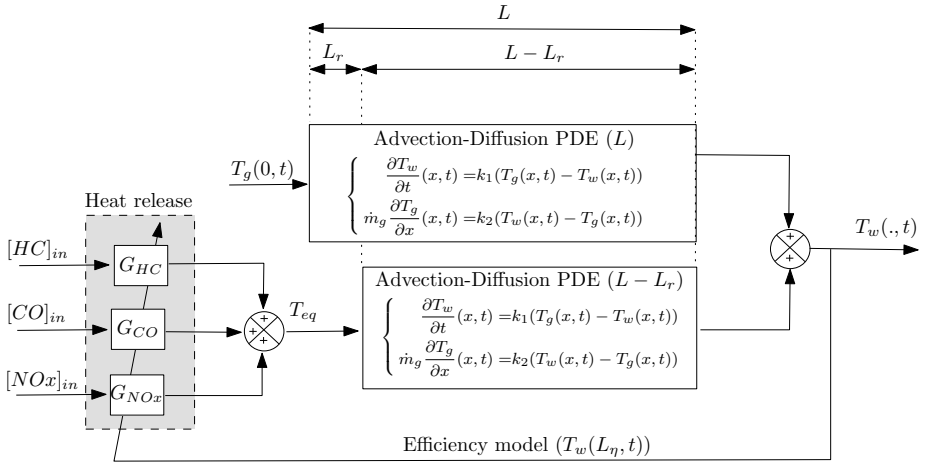

Fig. 6. Proposed catalyst temperature PDE model. The pollutant conversion effects (HC, CO and NO_x) are assimilated to a front of temperature T_{eq} propagating on a virtual length $L_\eta - L_r$, while the gas heating occurs on the complete length L_η. The model is also fed by the gas mass flow rate $\dot{m}_g$ which is not represented here for sake of clarity.

wall temperature at L_η[9], handling the potential variability of this position[10]. Yet, the equations presented above are not real-time compliant and therefore cannot be used on an embedded engine control strategy. For this reason, we study their low-frequency behavior in the following section to obtain a simple ordinary differential dynamics.

IV. Approaching the dynamics by an input-delay ordinary differential equation

In this section, we present a semi-lumped representation of the PDE model described earlier. We summarize this input-delay model by the following claim.

Claim 1: The wall catalyst temperature at position L_η can be efficiently represented as

$$T_w(L_\eta) = T_w^{th} + T_w^{\Psi} \tag{4}$$

where T_w^{th} satisfies

$$\tau(L_\eta, t)\frac{dT_w^{th}}{dt} = -T_w^{th}(t) + T_g(0, t - D(L_\eta, t)) \tag{5}$$

and T_w^{Ψ} satisfies

$$\tau(L_\eta - L_r, t)\frac{dT_w^{\Psi}}{dt} = -T_w^{\Psi}(t) + T_{eq}(0, t - D(L_\eta - L_r, t)) \tag{6}$$

T_{eq} is defined in (3), the time constant τ and the delay D are defined for $x \in [0, L]$ as

$$\begin{cases} \tau(x,t) = \dfrac{1}{k_1} + \nu\delta(x,t) & (7) \\ D(x,t) = (1-\nu)\delta(x,t) & (8) \end{cases}$$

with ν a given constant in $[0,1]$ and δ defined through the integral equation

$$\int_{t-\delta(x,t)}^{t} \frac{k_1}{k_2}\dot{m}_g(s)ds = x \tag{9}$$

[9]An effective length L_η was identified as the one of the first monolith on experimental data.

[10]Yet, in the following, for experimental validation, we also compute wall temperature estimates at other locations.

A. Comments

The relation (9) implicitly defines a transport delay through past values of the gas flow rate. It corresponds to a transport phenomenon occurring over a length x with a speed $\frac{k_1}{k_2}\dot{m}_g$ accordingly to a Plug-Flow assumption [16]. This time can be understood as a residence time into the monolith (see [3]). As the two main effects of the gas residence inside the monolith are transport and exchange with the monolith, it can reasonably be separated into a first order dynamics with a pure delay effect. The tuning parameter ν can be determined via dedicated tests and allows this model to qualitatively represent a relatively vast range of catalyst devices.

It is worth noticing that the catalyst temperature at any position $x \in [0, L]$ can also be computed by a similar procedure, provided one has value of the steady-state gains (correspondingly, $T_w(L_\eta, .)$ has to be calculated independently).

We now give some elements to explain why this claim is formulated.

B. Derivation of Claim 1

Based on the previous PDE model presented in Section III (and summarized in Fig. 6), one notices that the following claim, characterizing the "purely thermal" behavior of the PDE model (i.e. without chemical heat release), is equivalent to the previous one.

Claim 2: Assume $\Psi = 0$. In the range of low (time domain) frequencies, the distributed parameter model (1)-(2) can be approximated by the following set of first-order delayed equations

$$\forall 0 \le x \le L, \quad \tau(x,t)\frac{dT_w(x,t)}{dt} = -T_w(x,t) + T_g(0, t - D(x,t)) \tag{10}$$

with τ, D and δ defined respectively in (7), (8) and (9).

We now focus on giving some elements of background for this last claim.

1) Modeling the transport delay: By taking a spatial derivative of (1) with $\Psi = 0$, a time-derivative of (2) and matching terms with (1)-(2), one can obtain the decoupled equations, for all $x \in [0, L]$,

$$\begin{cases} \dot{m}_g(t)\dfrac{\partial^2 T_w}{\partial x \partial t} = -k_2 \dfrac{\partial T_w}{\partial t} - k_1 \dot{m}_g(t) \dfrac{\partial T_w}{\partial x} \\ \dot{m}_g(t)\dfrac{\partial^2 T_g}{\partial x \partial t} + \ddot{m}_g(t)\dfrac{\partial T_g}{\partial x} = -k_2 \dfrac{\partial T_g}{\partial t} - k_1 \dot{m}_g(t) \dfrac{\partial T_g}{\partial x} \end{cases}$$

where the first equation defining T_w can be reformulated using a spatial Laplace transform (operational calculus) to get

$$\forall t \geq 0\,, \quad (\dot{m}_g(t)p + k_2)\frac{d\hat{T}_w}{dt} = -k_1 \dot{m}_g(t) p \hat{T}_w(p,t)$$

This scalar system can be solved as

$$\hat{T}_w(p,t) = \exp\left(-\left[\int_{t_0}^{t} \frac{k_1 \dot{m}_g(s) p}{\dot{m}_g(s)p + k_2} ds\right]\right) \hat{T}_w(p, t_0)$$

where t_0 is such that $t_0 \leq t$.

The catalyst, as is visible from experimental data reported in Fig. 2(b), is relatively non-sensitive to high-frequencies. Consequently, by considering only low-level spatial frequencies (i.e., $\dot{m}_g p << k_2$ for any gas flow $\dot{m}_g$), the term below the integral can be substantially simplified[11]. Rewriting the resulting equation into the usual space domain gives

$$\forall x \in [0, L]\,, \quad T_w(x,t) = T_w\left(x - \left[\int_{t_0}^{t} \frac{k_1}{k_2} \dot{m}_s(s) ds\right], t_0\right)$$

Formally, one can define $\delta(x,t) \geq 0$ such that

$$x - \left[\int_{t-\delta(x,t)}^{t} \frac{k_1}{k_2} \dot{m}_s(s) ds\right] = 0$$

which is (9). Consequently, the wall temperature at abscissa x is formally delayed by

$$\forall x \in [0, L]\,, \quad T_w(x,t) = T_w(0, t - \delta(x,t)) \tag{11}$$

2) Obtaining a finite-dimensional first-order model: From there, it is possible to relate the dynamics under consideration to the gas inlet temperature. Consider for a moment that $\delta(x)$ is constant with respect to time. Then, writing (11) in the time Laplace domain, jointly with (1) for $x = 0$, one directly obtains for all $x \in [0, L]$

$$\hat{T}_w(x,s) = k_1 \frac{e^{-\delta(x)s}}{s + k_1} \hat{T}_g(0,s) \tag{12}$$

Finally, following the same considerations as previously, it is possible to only consider low frequencies ($s << 1$). By considering, following the considerations presented in [15],

$$e^{-\delta(x)s} \approx \frac{e^{-(1-\nu)\delta(x)s}}{\nu\delta(x)s + 1}$$

with a constant $\nu \in [0, 1]$, (12) rewrites for low frequencies

$$\hat{T}_w(x,s) = \frac{e^{-(1-\nu)\delta(x)s}}{\left(\frac{1}{k_1} + \nu\delta(x)\right)s + 1} \hat{T}_g(x,0)$$

[11]The exact relation between time and spatial frequencies remains to be rigorously explored.

By formally generalizing this relation to a time-varying residence time $\delta(x,t)$, one obtains the dynamics formulated in Claim 2.

From there, matching Claim 2 with the chemical heat release model proposed in Section III, one can deduce Claim 1.

C. Validation of the reduced input-delay model (4)-(9) on experimental data

To illustrate Claims 1- 2, simulation results of the temperature inside the wall catalyst at two different locations are pictured in Fig. 7 for the NEDC cycle considered previously. The proposed simplified dynamics (4)-(9) is pictured in red and compared both to the experimental measurements and to the numerical solution of the PDEs of Section III. The physical parameters have been kept similar to the one previously used and the tuning parameter have been chosen as $\nu = 0.4$[12]

The simulated temperature almost perfectly matches both the one computed with the PDE model and experimental data. It is worth observing that the inputs corresponding to this NEDC cycle (in particular the gas mass flow rate) are highly variable and that therefore this test case is challenging. As these performances are obtained for very demanding external conditions, one can reasonably expect similar behavior on different kinds of driving conditions.

D. Comments about the reduced input-delay model

The proposed model is accurate and simple enough to be implemented in real-time. One extra advantage of the proposed technique that is worth noticing is that it provides insight into the temperature everywhere inside the monolith. A lumped model (or 0D-model) like the one presented in [10] for example, cannot achieve this. Also worth noticing is the fact that aging of the catalyst can be accounted for by updating L_η.

V. Prediction-based light-off strategy

In this section, we use the proposed input-delay model of Section IV to determine the light-off temperature reaching time, i.e. the time when the efficiency of the catalyst is greater than 90 percent. With this aim in view, we consider simulation results on the US driving cycle, FTP, and compare three different open-loop controllers.

A. Compared light-off open-loop strategies

From a bird's eye view, the three considered strategies achieve the same task. When the catalyst is cold, the combustion efficiency is degraded to provide higher exhaust gas temperature. Then, at the light-off temperature reaching time, standard combustion is performed again. The difference between the three following techniques relies on the determination of this light-off switching time.

[12]This value was calibrated using the same experimental data that in the previous section to calibrate the physical parameters (cold engine, constant requested torque and engine speed). The parameter ν was adjusted during this calibration procedure to maximize the match between the PDE model and the reduced one on these data.

1) Strategy 1 : calibration using the water cooling system temperature

As the temperature sensor of the water cooling system is the only exhaust temperature sensor commercially embedded, the light-off temperature is usually calibrated from its measurement. For the engine under consideration for the presented experiments (Renault F4Rt) and a NEDC cycle, the temperature of the cooling system corresponding to light-off is 74^{o}C. The light-off switching time used with this technique is then the time where the water cooling temperature reaches this value.

2) Strategy 2, using the reduced input-delay wall temperature

This strategy uses the efficiency function previously calibrated, fed with the input-delay temperature model proposed in Section IV at length L_η. The light-off switching time directly results from this model.

3) Strategy 3, using the prediction-based wall temperature

This strategy also uses the efficiency function, but fed with a prediction of the temperature model at length L_η. Indeed, by exploiting the input-delay form of the model (4)-(9), the light-off switching time can be scheduled in advance.

In details (see [1]), assuming that the external conditions remain similar (i.e., for $s \in [t, t+D(x,t)]$, $\tau(x,s) = \tau(x,t)$), then it is possible to predict the future value of the wall temperature at time $t+D(L_\eta,t)$, i.e.

$$T_w^{pred}(L_\eta,t) = T_w^{th}(L_\eta, t+D(t)) + T_w^{\Psi}(L_\eta, t+D(t))$$

with

$$T_w^{th}(L_\eta, t+D(L_\eta,t)) = e^{-\frac{1}{\tau(L_\eta,t)}} T_w^{th}(L_\eta,t) + \frac{1}{\tau(L_\eta,t)} \int_{t-D(L_\eta,t)}^{t} e^{-\frac{1}{\tau(L_\eta,t)}(t-s)} T_g(0, t-D(L_\eta,s)ds$$

and $T_w^{\Psi}(L_\eta, t+D(t))$ computed similarly. This prediction is obtained integrating (4) between t and $t+D(L_\eta,t)$ starting with the current modeled temperature value. When this predicted temperature reaches the light-off temperature, optimal combustion can be performed.

More precisely, due to the delay variations, this prediction may not be accurate (i.e. the computed value $T_w^{pred}(L_\eta,t)$ may not be achieved exactly at time $t+D(L_\eta)$) but still provides information about the catalyst warming. Indeed, due to the delayed input, one can expect then that the gas temperature that are already heating the monolith are sufficient to achieve the desired warming. Therefore, it can be decided to turn off combustion timing shifting when such a point is reached.

B. Simulation comparison results

Simulation results have been performed on the first 510s of the FTP cycle, represented in Fig. 8(c) and corresponding to real driving conditions over a distance of approximately 6 km. The three different strategies have been tested. Corresponding catalyst wall temperature at length L_η, with respective light-off switching times, are pictured in Fig. 8(a). These switching times are also reported on Table II, with consumption gain increases, compared to Strategy 1[13].

First, one can easily notice that Strategy 2 and 3 considerably lower the light-off switching time, resulting into substantial consumption decrease (see Table II). For this reason, as a degraded combustion is performed longer, the temperature obtained with Strategy 1 is much most important than the two others after a certain lag (transport delay).

[13]For sake of clarity, pollutant emissions are not reported here. Their scale is similar on the three study cases. Yet, the validity of this evaluation would benefit from dedicated experimental tests.

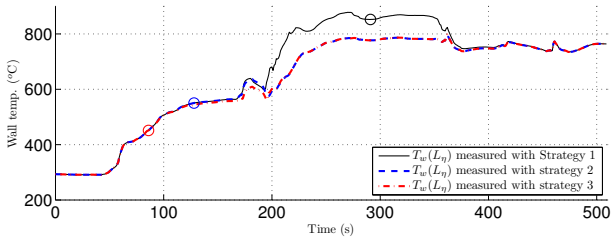

(a) Simulation results of the temperature at L_η for the three light-off strategy on a FTP cycle. The markers indicate the light-off time shifting.

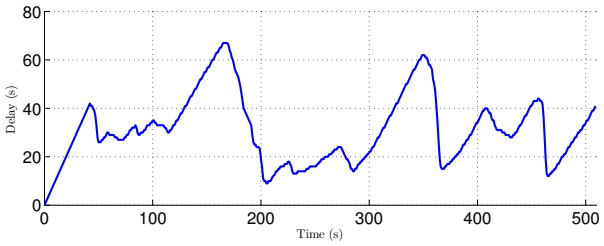

(b) Corresponding transport delay (Strategy 3)

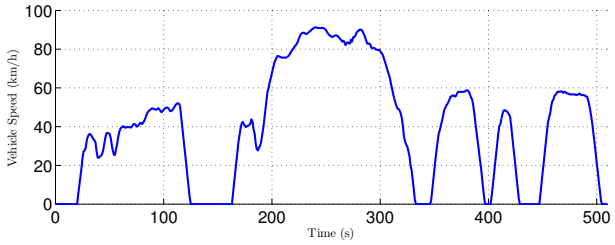

(c) Vehicle speed set-point.

Fig. 8. Comparison between the three control strategies applied on the first 510s of a FTP cycle with cold start.

	Time shifting [s]	Consumption reduction compared to Strategy 1 [%]
Strategy 1	291	0
Strategy 2	128	3.38
Strategy 3	86	3.46

TABLE II

COMPARISON OF THE LIGHT-OFF TIMINGS OBTAINED WITH THE THREE DIFFERENT STRATEGIES AND CONSUMPTION IMPACT (RELATIVE DIFFERENCE WITH THE CONSUMPTION OBTAINED USING STRATEGY 1).

The difference between the two switching times of Strategy 2 and 3 is compliant with the scale of the delay pictured in Fig. 8(b). On the time interval separating these two instants, one can observe on Fig. 8(a) that the two temperatures are similar. This is due to the delayed nature of the system. The strategy impact is only noticeable after that time: the temperature obtained with Strategy 2 is then higher than for Strategy 3. Strategy 3 has a moderate but positive impact on the consumption, without any prejudicial effects on the pollutant emissions.

VI. Conclusion

In this paper, a simple infinite dimensional model of the wall catalyst has been presented. A corresponding first-order input-delay reduction has been performed. Following the works presented in [12] on Diesel engines, the distributed heat generation resulting from pollutant conversion is represented as a second inlet temperature taking place on a virtual front inside the catalyst. This work has been shown to represent well the behavior of SI engine catalysts, thanks to the introduction of a closed-loop coupling on the conversion efficiency.

The reduced input-delay model suggests interesting control strategies for the light-off, which have been illustrated on simulations. In particular, comparing this strategy to the existing ones, this strategy enables to detect light-off independently on the driving cycle. Further experiments are needed to evaluate these potential merits. Another direction of work is the evaluation of the robustness of this model to input estimation errors.

Acknowledgment

The authors are thankful to Olivier Lepreux for fruitful discussions and advice and to Sopheaktra Kim, ENSTA ParisTech undergraduate student, who carried out substantial model developments during an internship.

References

[1] Z. Artstein. Linear systems with delayed controls: a reduction. *IEEE Transactions on Automatic Control*, 27(4):869–879, 1982.

[2] SF Benjamin and CA Roberts. Automotive catalyst warm-up to light-off by pulsating engine exhaust. *International Journal of Engine Research*, 5(2):125–147, 2004.

[3] PV Danckwerts. Continuous flow systems: distribution of residence times. *Chemical Engineering Science*, 2(1):1–13, 1953.

[4] C. Depcik and D. Assanis. One-dimensional automotive catalyst modeling. *Progress in energy and combustion science*, 31(4):308–369, 2005.

[5] L. Eriksson. Mean value models for exhaust system temperatures. In *Proc. of the Society of Automotive Engineering World Congress*, number 2002-01-0374, 2005.

[6] H. Fu, X. Chen, I. Shilling, and S. Richardson. A one-dimensional model for heat transfer in engine exhaust systems. In *Proc. of the Society of Automotive Engineering World Congress*, number 2005-01-0696, 2005.

[7] L. Guzzella and C. H. Onder. *Introduction to modeling and control of internal combustion engine systems*. Springer Verlag, 2010.

[8] J. B. Heywood. *Internal combustion engine fundamentals*. McGraw-Hill New York, 1988.

[9] U. Kiencke and L. Nielsen. *Automotive control systems*. Springer-Verlag, Berlin, 2000.

[10] D. Kum, H. Peng, and N. K. Bucknor. Optimal energy and catalyst temperature management of plug-in hybrid electric vehicles for minimum fuel consumption and tail-pipe emissions. *IEEE Transactions on Control Systems Technology*, 21(99):14–26, 1999.

[11] P. M. Laing, M. D. Shane, S. Son, A. A. Adamczyk, and P. Li. A simplified approach to modeling exhaust system emissions: SIMTWC. *SAE paper*, -:01–3476, 1999.

[12] O. Lepreux. *Model-based temperature control of a Diesel oxidation catalyst*. PhD thesis, MINES Paristech, 2010.

[13] L. Olsson and B. Andersson. Kinetic modelling in automotive catalysis. *Topics in catalysis*, 28(1):89–98, 2004.

[14] A. Onorati, G. D'Errico, and G. Ferrari. 1D fluid dynamic modeling of unsteady reacting flows in the exhaust system with catalytic converter for SI engines. *SAE Transactions*, 109(2000-01-0210):89–103, 2000.

[15] L. Pekar and E. Kureckova. Rational approximations for time-delay systems: case studies. In *Proceedings of the 13th WSEAS international conference on Mathematical and computational methods in science and engineering*, pages 217–222. World Scientific and Engineering Academy and Society (WSEAS), 2011.

[16] R. H. Perry, D. W. Green, and J. O. Maloney. *Perry's chemical engineers' handbook*, volume 7. McGraw-Hill New York, 1984.

[17] C. P. Please, P. S. Hagan, and D. W. Schwendeman. Light-off behavior of catalytic converters. *SIAM Journal on Applied Mathematics*, 54(1):72–92, 1994.

[18] K. Ramanathan, D. H. West, and V. Balakotaiah. Optimal design of catalytic converters for minimizing cold-start emissions. *Catalysis today*, 98(3):357–373, 2004.

[19] J. Vardi and W. F. Biller. Thermal behavior of exhaust gas catalytic convertor. *Industrial & Engineering Chemistry Process Design and Development*, 7(1):83–90, 1968.

[20] L. C. Young and B. A. Finlayson. Mathematical models of the monolith catalytic converter. *AIChE Journal*, 22(2):343–353, 1976.

Appendix

In this appendix, we provide a more detailed modeling of the thermal exchanges occurring in the catalyst, from which (1)-(2) is a simplification. Following [4], a thermal balance of the gas leads to the equation

$$\rho_g A_g C p_g \frac{\partial T_g}{\partial t} + \dot{m}_g C p_g \frac{\partial T_g}{\partial x} = h_I P_I (T_w(x,t) - T_g(x,t)) \quad (13)$$

where the first term on the left hand side accounts for the gas energy storage, the second one for transport and the right-hand term for convective exchanges. A similar balance for the wall yields

$$\begin{aligned}\rho_w A_w C p_w \frac{\partial T_w}{\partial t} =& \lambda_w \frac{\partial^2 T_w}{\partial x^2} + \sum_{i=1}^{N} R_i h_i + h_I P_I (T_g(x,t) - T_w(x,t)) \\ &+ h_O P_O (T_{amb} - T_w(x,t)) \end{aligned} \quad (14)$$

where the left-hand side still accounts for the energy storage and the right-hand side represents respectively: i) the conduction/diffusion inside the monolith; ii) the enthalpy flow of the N chemical reactions occurring inside the catalyst (mainly, $N = 3$); iii) the exchange respectively with the gas and the atmosphere.

One can notice that, following [12], no transport occurs in the (solid) wall. In more details, a mass balance of the species in presence can be established. The species concentrations inside the monolith are necessary to determine the reaction terms R_i in the enthalpy flows. Two additional equations per species are also necessary (one for the gas and one for the monolith, see [2] [13]).